Published OnlineFirst February 6, 2020; DOI: 10.1158/0008-5472.CAN-19-2578

Cancer Cell–Derived Matrisome Proteins Promote Metastasis in Pancreatic Ductal Adenocarcinoma

Chenxi Tian[1], Daniel Öhlund[2,3,4], Steffen Rickelt[1], Tommy Lidström[3,4], Ying Huang[1], Liangliang Hao[1], Renee T. Zhao[1], Oskar Franklin[5], Sangeeta N. Bhatia[1,6], David A. Tuveson[2], and Richard O. Hynes[1,6]

ABSTRACT

The prognosis for pancreatic ductal adenocarcinoma (PDAC) remains poor despite decades of effort. The abundant extracellular matrix (ECM) in PDAC comprises a major fraction of the tumor mass and plays various roles in promoting resistance to therapies. However, nonselective depletion of ECM has led to poor patient outcomes. Consistent with that observation, we previously showed that individual matrisome proteins derived from stromal cells correlate with either long or short patient survival. In marked contrast, those derived from cancer cells correlate strongly with poor survival. Here, we studied three cancer cell–derived matrisome proteins that are significantly overrepresented during PDAC progression, AGRN (agrin), SERPINB5 (serine protease inhibitor B5), and CSTB (cystatin B). Using both overexpression and knockdown experiments, we demonstrate that all three are promoters of PDAC metastasis. Furthermore, these proteins operate at different metastatic steps. AGRN promoted epithelial-to-mesenchymal transition in primary tumors, whereas SERPINB5 and CSTB enhanced late steps in the metastatic cascade by elevating invadopodia formation and *in vivo* extravasation. All three genes were associated with a poor prognosis in human patients and high levels of SERPINB5, secreted by cancer cells and deposited in the ECM, correlated with poor patient prognosis. This study provides strong evidence that cancer cell–derived matrisome proteins can be causal in promoting tumorigenesis and metastasis and lead to poor patient survival. Therefore, compared with the bulk matrix, mostly made by stromal cells, precise interventions targeting cancer cell–derived matrisome proteins, such as AGRN, SERPINB5, and CSTB, may represent preferred potential therapeutic targets.

Significance: This study provides insights into the biological roles of cancer cell–derived matrisome proteins in PDAC and supports the notion that these proteins are protumorigenic and better therapeutic targets.

Introduction

Prognosis for pancreatic ductal adenocarcinoma (PDAC) remains dismal, with 5-year survival rate being less than 9% (1). PDAC is characterized by a pronounced resistance to radiation, cytotoxic agents, and targeted and immunotherapies (2). PDAC has highly desmoplastic stroma, constituting a major fraction (up to 90%) of the tumor mass and composed of a variety of nonneoplastic cell types and extracellular matrix (ECM). The chemo- and radiotherapeutic resistance of PDAC is thought to be mediated, at least in part, by its prominent ECM, which compresses blood vessels, resulting in inefficient drug delivery and promoting survival through integrin-mediated signaling pathways (3). However, nonselective depletion of stroma by targeting the ECM-inducing Hedgehog signaling pathway (4) or depleting α-smooth muscle actin–positive fibroblast cells (5) in mice resulted in poorly differentiated cancer cells and poor survival, despite successful depletion of stroma and enhanced drug uptake. Similarly, clinical trials targeting metastatic PDAC using Smoothened inhibitor blockade of Hedgehog signaling were halted because of paradoxical acceleration of disease progression (6). Thus, the prominent ECM in PDAC appears to have a dual nature, at times even restraining pancreatic cancer progression.

During cancer progression, ECM deposited by both cancer cells and various stromal cells (7, 8) plays both biophysical and biochemical roles to regulate malignant cell behaviors. For example, in the tumor microenvironment, ECM proteins can directly promote oncogenic transformation and metastasis, and influence stromal cell behaviors, such as angiogenesis and inflammation, resulting in formation of a protumorigenic microenvironment (9). In distant organs, ECM proteins have been shown to contribute to metastatic niches that maintain cancer cell stemness and enable cancer cell outgrowth (10, 11). The matrisome is defined as both core ECM proteins, including collagens, glycoproteins and proteoglycans, and ECM-associated proteins, such as ECM regulators (e.g., proteases and their inhibitors, cross-linking agents), ECM-affiliated proteins (e.g., mucins, lectins, annexins), and secreted factors (e.g., growth factors, chemokines; ref. 8). We and others have used LC/MS-MS to define the matrisome compositions in mouse tumorigenic models, as well as human tumors (12), and such studies have revealed previously unknown, functionally relevant promoters of cancer progression.

In a recent study, we applied quantitative mass spectrometry–based proteomic approaches to systematically profile the composition and dynamics of ECM proteins during PDAC progression in both mouse genetic PDAC models and human patient samples (13). We identified over 200 matrisome proteins that are significantly overrepresented in PDAC compared with normal pancreas in human samples and assigned cancer cell versus stromal origin to a majority of them. We

[1]Koch Institute for Integrative Cancer Research, Massachusetts Institute of Technology, Cambridge, Massachusetts. [2]Cold Spring Harbor Laboratory, Cold Spring Harbor, New York. [3]Department of Radiation Sciences, Umeå University, Umeå, Sweden. [4]Wallenberg Centre for Molecular Medicine, Umeå University, Umeå, Sweden. [5]Department of Surgical and Perioperative Sciences, Umeå University, Umeå, Sweden. [6]Howard Hughes Medical Institute, Chevy Chase, Maryland.

Note: Supplementary data for this article are available at Cancer Research Online (http://cancerres.aacrjournals.org/).

Corresponding Author: Richard O. Hynes, Massachusetts Institute of Technology, 77 Massachusetts Ave, 76-361D, Cambridge, MA 02139. Phone: 617-253-6422; Fax: 617-253-8357; E-mail: rohynes@mit.edu

Cancer Res 2020;80:1461–74

doi: 10.1158/0008-5472.CAN-19-2578

Published OnlineFirst February 6, 2020; DOI: 10.1158/0008-5472.CAN-19-2578

found that high levels of ECM proteins derived from tumor cells, rather than those exclusively produced by stromal cells, tend to correlate with poor patient survival, while stromal cell–derived ECM proteins can either positively or negatively correlate with survival. That study supported the hypothesis that PDAC stroma has a dual role and argued (i) against nonselective depletion of stroma, and (ii) that cancer cell–derived matrisome proteins may be potential therapeutic targets.

In this study, we selected three cancer cell–derived matrisome proteins that are overrepresented in PDAC (AGRN, SERPINB5, and CSTB) and performed functional studies *in vivo*. These experiments revealed their functions in promoting different steps of metastasis. We also showed that high expression levels of all three genes correlate with poor patient survival. These results demonstrate that the detailed proteomic analysis of PDAC tumor ECM can identify clinically relevant ECM proteins promoting tumor development and metastasis, which are potential candidates for future focused therapeutic interventions.

Materials and Methods

Cell line maintenance and mouse strains

The MIT Animal Care and Use Committees reviewed and approved all animal studies and procedures. NOD/SCID/IL2Rγ-null (NSG) mice were used throughout the study (Jackson Laboratory). The human pancreatic adenocarcinoma cell lines AsPC1 and BxPC3 were purchased from ATCC, where they were tested and authenticated. The human CAF cell line hT1 was published previously (14). AsPC1 was cultured in RPMI1640 medium (Thermo Fisher Scientific) and the other cell lines were cultured in HyClone high-glucose DMEM (Thermo Fisher Scientific), supplemented with 10% FBS (Invitrogen) at 37°C in a 5% CO_2 incubator.

Generation of *in vivo* selected BxPC3 cell lines

BxPC3 G1.1 cells were *in vivo* selected from parental BxPC3 cells through three rounds of metastasis in 8- to 10-week-old NOD/SCID/IL2Rγ-null mice (Jackson Laboratory). For each round of selection, 1×10^6 cells in 50 μL PBS were implanted into the pancreas; 4 weeks later, lung metastatic nodules were removed aseptically and treated with type I collagenase (17018029, Thermo Fisher Scientific) following the product manual and cells were grown *in vitro*. The resulting cells were implanted in the pancreas for the next round of selection. For ease of quantification, all the cells were rendered Zsgreen-positive by retroviral infection with MSCV-puromycin-IRES-Zsgreen.

CRISPR activation

AsPC1 cells stably expressing dCas9-VP64-Blast (Addgene #61425) and MS2-P65-Hygro (Addgene #61426) were generated through sequential lentiviral transduction and selection with blasticidin and hygromycin, respectively (15). The resulting AsPC1 cells were then transduced with lentiviral vector (Lenti-sgRNA-MS2-Zeocin; Addgene #61427) inserted with gRNA targeting promoter sequences of each gene and subsequently zeocin-selected to generate the final cell lines stably overexpressing genes of interest. The target gRNA sequences were designed using the SAM website (http://sam.genome-engineering.org). We tested 5 to 10 different gRNAs and selected two gRNAs that led to the best overexpression of the genes of interest. The gRNAs selected were as follows, with PAM sequences in bold:

CSTB 1 TTTCCGGGCGCCGAGTCACA**CGG**;
CSTB 2 CGGAAAGACGATACCAGCCC**CGG**;
AGRN 1 AGGGGGAGGAGGAGGGCGCG**GGG**;
AGRN 2 GACAGGACGGGACGCAGCTC**CGG**;
SERPINB5 1 AGCTGCCAAGAGGCTTGAGT**AGG**;
SERPINB5 2 ATTGTGGACAAGCTGCCAAG**AGG**.

CRISPR inactivation

BxPC3 G1.1 cells were transduced with pHR-TRE3G-KRAB-dCas9-P2A-Blast lentivirus, which is modified from a construct (Addgene #60954) by replacing SFFV promoter with a doxycycline-inducible promoter TRE3G and mCherry with blasticidin sequence, and selected with blasticidin (16). The cells were then transduced with pHR-SFFV-TET3G at 1:10 dilution without selection (kind gift from Luke Gilbert in the Weissman lab, University of California, San Francisco, San Francisco, CA). The resulting cells were then transduced with lentiviral vector that is modified lentiGuide-Puro (lentiGuide-Puro, Addgene #52963) by replacing puro with tdTomato sequence and sorted by FACS for cells positive for tdTomato. The gRNA sequences were targeted against -50 to 200 bp of the transcription start site of each gene (16). We tested 5 to 15 different gRNAs in the presence of doxycycline and selected gRNAs that knocked down the genes of interest to the greatest extent. The gRNAs selected are as follows, with PAM sequences in bold:

CSTB 1 CGCCGCCAAGATGATGTGCG**GGG**;
SERPINB5 1 AGCTGCCAAGAGGCTTGAGT**AGG**;
SERPINB5 2 ACACGGTCGCCTCCACATCC**AGG**
AGRN 1 GGTGCTCACCGGGACGGTGG**AGG**;
AGRN 2 GTCCAGTCCCGTCCCCGGCG**CGG**.

Both control and experimental mice were fed with DOX diet (Bio-serv) throughout the experiment.

Orthotopic and tail-vein implantation

For CRISPR-SAM activation and CRISPR inactivation experiments, 1×10^5 cells in 50 μL PBS were injected into pancreata of 8- to 10-week-old NSG mice (Jackson Laboratory). Tumors were harvested 6 (CRISPR inactivation) or 10 (CRISPR-SAM activation) weeks postinjection. For tail-vein injection, 5×10^4 cells in 100 μL PBS were injected into the lateral tail vein of 8- to 12-week-old NSG mice. The mice were sacrificed 6 weeks later and lungs were imaged by fluorescence microscopy and then fixed overnight with 4% paraformaldehyde solution in PBS (Santa Cruz Biotechnology). Samples were kept in 70% ethanol prior to embedding and sectioning. All procedures were performed according to an animal protocol approved by MIT's Department of Comparative Medicine and Committee on Animal Care.

Quantification of metastases

ZsGreen-positive metastatic load was quantified using ImageJ in the left pulmonary lobe. Metastasis load in the left lobe is representative of all lung lobes. Thresholding method was chosen for each experiment. Manual curation was applied when necessary. Two-tailed Student *t* test was performed to evaluate the statistical significance of the results.

Extravasation assay

Cells (2×10^5 in 100 μL PBS) were injected via lateral tail vein into NSG mice. Twenty-four hours after injection, mice were euthanized and lungs were collected after inflation with 4% paraformaldehyde solution and 0.3% Triton X-100. Fixed lungs were cut into 0.5-mm slices and stained with anti-CD31 (5533070, BD Biosciences) and Alexa 594–conjugated goat anti-rat IgG (Molecular Probes). Scoring was done blindly. Images were taken with a Nikon A1R laser-scanning confocal microscope using a 40× objective and tumor cells were scored as intravascular or extravascular.

Published OnlineFirst February 6, 2020; DOI: 10.1158/0008-5472.CAN-19-2578

Immunohistochemistry

Tissues (lungs and pancreas) were fixed in 4% paraformaldehyde solution or 10% neutral-buffered formalin at room temperature overnight and paraffin-embedded following standard procedures. Consecutive sections were prepared using a Leica RM2255 rotary microtome (Leica Biosystems) and dried at 60°C for 1 hour. The sections were then dewaxed and rehydrated before staining with hematoxylin and eosin (H&E) or treatment with heat-induced epitope-retrieval (HIER) using a decloaking chamber (Biocare Medical) prior to immunostaining. The sections were incubated in 10 mmol/L sodium citrate (pH6.0) or 10 mmol/L Tris (pH 9.0) buffered solutions containing 0.05% Tween at 120°C for 2 minutes using a pressure cooker (HIER step). If needed, additional enzyme treatment using pepsin was included. To obtain consistent and reliable staining on all tissues investigated, an automated staining system (LabVision Autostainer 360, Thermo Fisher Scientific) was used. To destroy all endogenous peroxidase and alkaline phosphatase activity in the tissue, the sections were subsequently pretreated using BLOXALL endogenous enzyme blocking solution (Vector Laboratories) for 10 minutes. After a blocking step with normal serum, the sections were incubated with the individual primary antibodies for 1 hour followed by secondary ImmPRESS polymer detection systems (Vector Laboratories) according to the manufacturer's protocol. The Vulcan Fast Red Chromogen Kit 2 (red staining; Biocare Medical) and the DAB Quanto Substrate System (brown staining; Thermo Fisher Scientific) were applied as substrates. For multicolor IHC stainings, following HIER and blocking steps, the individual antibodies were incubated consecutively using the chromogens indicated above. For counterstaining, hematoxylin was used. Primary antibodies used were: AGRN (Novus Biologicals, NBP1-90209), CDH1 (BD Biosciences, 610181), CSTB (Abcam, ab53725), LMNA (human specific; Abcam, ab108595), SERPINB5 (Origene, TA-322980), VIM (human specific; Leica Biosystems, NCL-L-VIM-V9), and ZEB1 (Sigma-Aldrich, HPA027524).

Immunoblotting of tumor samples, cells, and cell culture media

Tumor samples were lysed in Laemmli buffer, proteins were separated by SDS-PAGE (4%–20% gradient gel from Bio-Rad), and immunoblotting was performed using the following antibodies: GAPDH (Millipore, MAB374), AGRN (Novus Biologicals, NBP1-90209), SERPINB5 (Origene, TA-322980), CSTB (Abcam, ab53725). Chemiluminescence development was done using Tanon 5200CE. To collect cell culture media for immunoblotting, freshly confluent control BxPC3 cells and those overexpressing SERPINB5 or CSTB by CRISPR-SAM method are cultured in CHO media (Hyclone) for 2 days. The supernatant was high-speed centrifuged to remove cell debris and concentrated 10-fold by Amicon centrifugal filters (EMD Millipore).

Reverse transcription and quantitative real-time PCR

RNA was isolated from cell or tumor lysates using an RNeasy kit (Qiagen) and cDNA was synthesized by reverse transcription using the First-Strand cDNA Synthesis Kit (Promega). qPCR reactions were performed using Bio-Rad SYBR Green Supermix (Bio-Rad) according to the manufacturer's instructions. qPCR results were analyzed in Microsoft Excel. Student *t* test was performed to evaluate the statistical significance of differences between groups. Human and murine PCR primers used are listed in Supplementary Table S1.

RNA *in situ* hybridization

Formalin-fixed paraffin-embedded tissue was sectioned (4 μm) and analyzed for SERPINB5 and Cytokeratin-19 (*KRT19*) expression using ViewRNA ISH Tissue Assay Kit (Thermo Fisher Scientific), with probes against *SERPINB5* (VA1-12247-VT) and cytokeratin-19 (VA6-10947-VT) (Thermo Fisher Scientific), according to the manufacturer's protocol. In short, tissue was deparaffinized in xylene and 100% ethanol. The sections were pretreated for 10 minutes at 90°C–95°C, followed by protease digestion for 10 minutes at 40°C and then fixed in 10% normal buffered formalin, followed by hybridization with the target probes against SERPINB5 and KRT19 for 2 hours in 40°C. The sections were stored overnight in storage buffer before proceeding with signal amplification and detection. The sections were preamplified for 25 minutes at 40°C followed by amplifier hybridization for 15 minutes at 40°C, followed by incubation with label probes at 40°C for 15 minutes and addition of substrate. FastRed label probe and substrate incubation was performed first. Sections were then counterstained in Gil hematoxylin, dipped in 0.01% ammonium hydroxide followed by DAPI staining (1 μg/mL for 10 minutes). Slides were mounted with Prolong gold antifade mountant with DAPI (Thermo Fisher Scientific). The confocal images were taken on a Zeiss LSM 710 microscope and the IHC images were scanned on the 3DHISTECH Pannoramic 250 flash III.

Quantification of double-color IHC images

Double-color IHC images were taken at 20× (ZEB1) and 10× (VIM and CDH1) to cover all the regions in each tumor. A macro was written to perform image quantification in ImageJ. Specifically, color deconvolution was used to separate the red and brown channels, and then the two channels were thresholded and outlined with the "Yen" algorithm. Then, for each nucleus that is positive for LMNA, the program decides if the cell is also positive in the second channel. Finally, the positive cell fraction is calculated. For each tumor, at least 2,000 cells covering the entire tumor region were quantified. Two-tailed Student *t* test was performed to evaluate the statistical significance of the results.

Tissue samples and tissue microarray construction

The tissue microarray (TMA) was constructed from cancer specimens of patients that underwent surgery for PDAC between 1990 and 2009 at Umeå University Hospital (Umeå, Sweden). All participating individuals provided written informed consent. The study was conducted in accord with the Helsinki Declaration of 1975 and was approved by the regional research ethics board of northern Sweden (Dnr. 09-175M/2009-1378-31). Core areas of 1 mm in diameter were first selected by an experienced pathologist, then drilled and placed on recipient blocks using a TMA Grand master machine (3DHISTECH). Three cores were included from each primary tumor ($n = 75$) and 1–3 cores from metastatic lymph nodes ($n = 32$). The cores were coded and randomly placed on the recipient blocks. Clinical data were retrieved from hospital charts. Scoring of at least two tissue cores per patient was required for comparison of staining intensity to survival. The observers were blinded for the clinical information during analysis of tissue staining. Normal pancreatic tissue was collected as control from patients undergoing pancreatic surgery for nonmalignant conditions ($n = 4$).

IHC Scoring for human TMA

IHC staining intensity was analyzed by two independent investigators. Stromal and epithelial intensity were semiquantitatively scored (1 = low intensity, 2 = moderate intensity, 3 = high intensity, 4 = very high intensity). When scoring differed between investigators, the mean of the differing scores was used. Patients were divided into high (intensity score > 2) and low intensity (intensity score ≤ 2) groups,

Published OnlineFirst February 6, 2020; DOI: 10.1158/0008-5472.CAN-19-2578

and their survival was compared. Mantel–Cox test was used to calculate *P* values.

Gelatin degradation assay and immunofluorescence staining

To label coverslips with fluorescent gelatin, 18 mm circular no. 2 cover glasses (VWR) were washed with a 2:1 mixture of nitric to hydrochloric acid for 2 hours, rinsed with 70% ethanol, then coated with 50 μg/mL poly-D-lysine for 20 minutes and fixed with 0.5% glutaraldehyde for 15 minutes. After washing with PBS, coverslips were then coated with Alexa Fluor 594-gelatin (Thermo Fisher Scientific, A20004) mixed with 2% sucrose. Alexa Fluor 594-gelatin was generated following a protocol described elsewhere (17). Coverslips were then coated with 20 μg/mL fibronectin (Advanced BioMatrix) and quenched with 5 mg/mL sodium borohydride (Sigma). Thirty-thousand cells were added to each gelatin-coated coverslip. AsPC1 cells were fixed 20 hours after plating with 4% paraformaldehyde and stained with 0.5 μg/mL DAPI (Thermo Fisher Scientific). TKS5 immunofluorescence staining followed a published protocol (18). In short, AsPC1 cells were plated on gelatin-coated coverslips that were prepared using the same method as for the gelatin degradation assay for 20 hours. Then, the cells were fixed with 4% paraformaldehyde, blocked, and incubated first with 2 mg/mL of TKS5 antibody (clone 13H6.3, Millipore Sigma, MABT336) and then with Alexa Fluor-488 or -594 anti-mouse IgG (Thermo Fisher Scientific). All images for gelatin degradation assay and TKS5+ invadopodia quantification assay were taken with a Nikon A1R laser-scanning confocal microscope using a 40× objective and then quantified with ImageJ. For each cell line, at least 20 fields were counted with at least 16 cells per field.

Proliferation assay

The assays were performed in the Incucyte Zoom System (Essen Bioscience). For proliferation, 10,000 cells were seeded in triplicate into 96-well plate to reach 10% confluence. Phase-contrast images were captured every 3 hours to calculate percent confluency. At least 10 fields were quantified for each cell line. *P* values were individually calculated by Student *t* test for the last 12 hours (last four time points), and then were corrected for multiple testing using the Benjamini–Hochberg method. The highest adjusted *P* value among the four points for each cell line are represented by asterisk(s) (*, $P < 0.05$; **, $P < 0.01$; ***, $P < 0.001$; ****, $P < 0.0001$; ns, not significant).

Survival analysis

Gene expression and clinical data for human pancreatic ductal adenocarcinoma (TCGA) were downloaded from cBioPortal (19). Gene expression data were Z-score normalized. For each gene, we calculated the log-rank *P* values and HRs by determining the overall survival differences in categorized patients using quartile expression values (top vs. bottom quartile). The Cox regression analyses were done using the R package OIsurv.

Recombinant protease and cell lysate substrate cleavage assay

Protease substrates with fluorescence (FAM) and quencher (CPQ2) were synthesized by CPC Scientific Inc. Peptide sequences are as following: Q3, PVGLIG; Q6, PLGLRSW; PQ19, PVPLSLVM; PQ2, GGSGRSANAK. In recombinant protease cleavage assay, protease vendor and buffer conditions were: MMPs (Enzo; 50 mmol/L TRIS, pH 7.5, 10 mmol/L $CaCl_2$, 300 mmol/L NaCl, 20 μmol/L $ZnCl_2$, 0.02% Brij-35, 1% BSA); ADAMs (Enzo; 10 mmol/L HEPES, pH 7.4, 100 mmol/L NaCl, 0.01% Brij-35, 1% BSA); uPA (R&D Systems; 50 mmol/L Tris, 0.01% Tween 20, pH 7.4, 1% BSA); Cathepsin B (R&D Systems; 25 mmol/L MES, 5 mmol/L DTT, pH 5.0); Cathepsin D (R&D Systems; 0.1 mol/L NaOAc, 0.2 mol/L NaCl, pH 3.5); Cathepsin E (R&D Systems; 0.1 mol/L NaOAc, 0.5 mol/L NaCl, pH 3.5); Cathepsin K (Enzo; 50 mmol/L NaOAc, 1 mmol/L DTT, pH 5.5); Cathepsin L (R&D Systems; 50 mmol/L MES, 5 mmol/L DTT, 1 mmol/L EDTA, 0.005% (w/v) Brij-35, pH 6.0). In the cell lysates cleavage assay, cell lysates were freshly prepared in lysis buffer (1%NP-40, 0.15 mol/L NaCl, 10 mmol/L Tris, pH 7.5) with and without 1 mmol/L EDTA at 2 mg/mL prior to assay. Assays were performed in the 384-well plate in triplicate in enzyme-specific buffer with peptides (1 μmol/L) and proteases (40 nmol/L) in 30 μL at 37°C. Fluorescence was measured at Ex/Em 495/535 nm using a Tecan Infinite 200 Pro Microplate Reader (Tecan). Signal increase at 60 minutes was monitored at 2-minute interval across conditions. Initial cleavage rate was calculated using ImageJ. Two-tailed *t* test was performed to compare the overexpressing cell lysates to the control cell lines. Independent validation on the four peptide substrates was also published elsewhere (T3 is Q3, T6 is Q6, T56 is PQ19; ref. 20).

Results

AGRN, SERPINB5, and CSTB are upregulated in PDAC and correlate with poor patient survival

We previously used proteomics to identify matrisome proteins overrepresented during PDAC progression and found that high expression of many cancer cell–derived matrisome proteins correlates with poor survival (published results summarized and illustrated in **Fig. 1A**; ref. 13). We wished to test directly whether ECM proteins differing between normal pancreas and PDAC might play causal roles during PDAC tumor progression. We selected three cancer cell–derived proteins (AGRN, agrin; SERPINB5, serine protease inhibitor Family Member B5 or Maspin; CSTB, cysteine protease inhibitor B or cystatin B) based on the following criteria: (i) significantly overrepresented and abundantly present in human PDAC MS analyses (**Fig. 1B–D**; Supplementary Table S2); (ii) expressed exclusively or mostly by the cancer cells (**Fig. 1A**); (iii) correlated with poor patient overall survival when highly expressed (**Fig. 1E–G**); and (iv) have not previously been functionally studied in PDAC progression and metastasis by *in vivo* experiments (Supplementary Table S2). We confirmed that their RNA expression levels are increased during PDAC progression in the KPC mouse model (**Fig. 1H–J**). By IHC, we also confirmed that the expression levels of all three proteins are higher in PDAC compared with normal pancreas in both human and mouse samples/tissues (**Fig. 1K–M**). AGRN is a heparan sulfate basal-lamina glycoprotein, and we observed it expressed predominantly in the basement membrane surrounding the diseased epithelial compartment (**Fig. 1K**). SERPINB5 and CSTB, on the other hand, are more diffusely localized, both intracellularly and extracellularly (**Fig. 1L** and **M**). Besides AGRN, SERPINB5, and CSTB, there are a few other proteins that also fit our selection criteria, including MXRA5, LMAN1 and S100A16, which could be interesting proteins for future studies (Supplementary Table S2).

Knockdown of AGRN, SERPINB, and CSTB in tumor cells reduces tumor growth and *in vivo* metastasis

To investigate their functions, we first used a CRISPR-driven inactivation system (16) to suppress expression of each of the three genes. The inactivation was performed in an *in vivo* selected highly lung-metastatic BxPC3 cell line, whose parental BxPC3 line has high expression levels for all three genes, based on data from the Cancer Cell

Published OnlineFirst February 6, 2020; DOI: 10.1158/0008-5472.CAN-19-2578

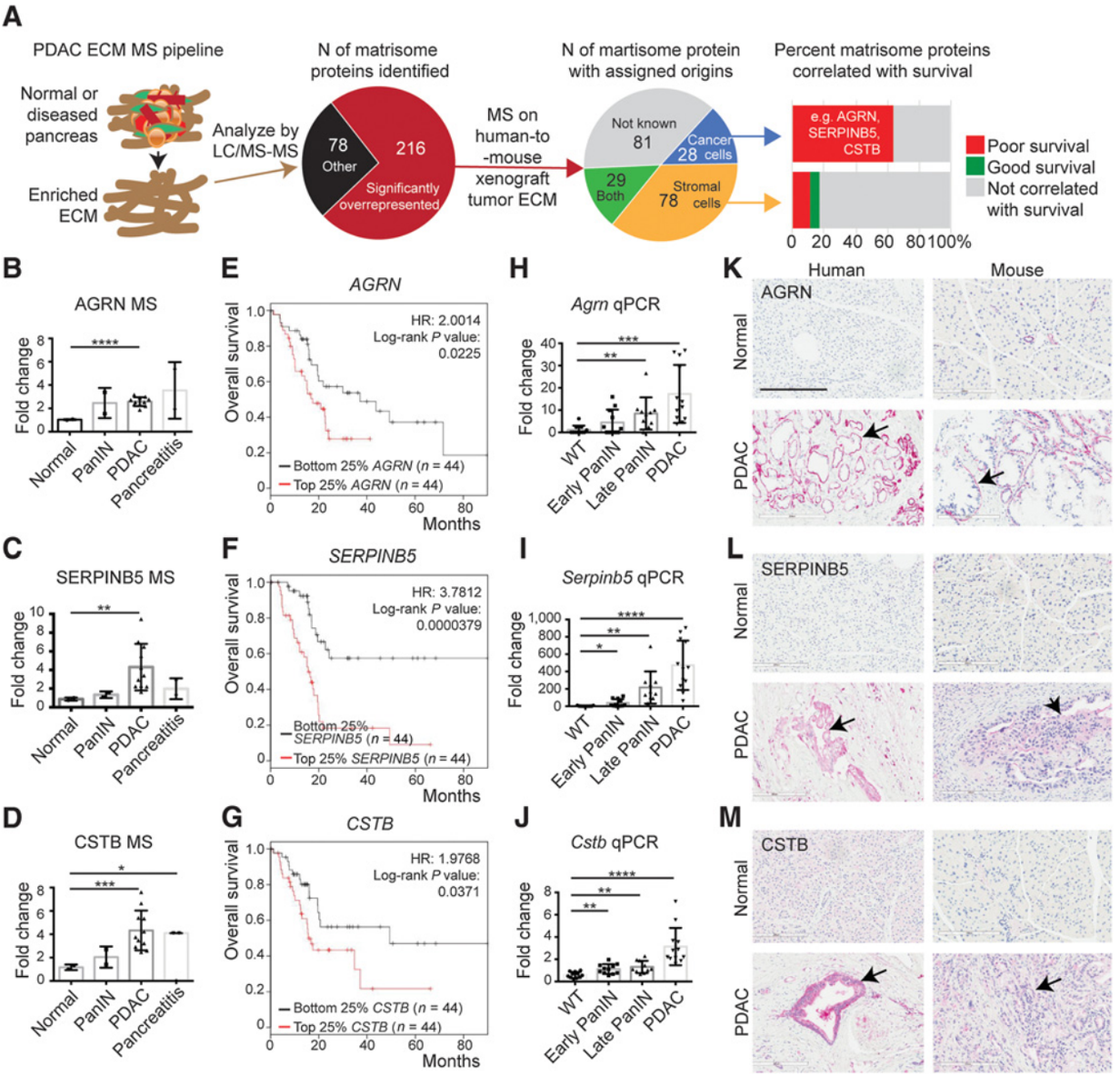

Figure 1.

Expression of AGRN, SERPINB5, and CSTB in PDAC and correlation with patient survival. **A,** A proteomic pipeline was used to identify overrepresented matrisome proteins in PDAC, and these proteins were then assigned as originating from human (cancer cell) or mouse (stroma) by MS analyses of human-to-mouse xenograft tumor ECM (13). Analyses of correlations with patient survival of individual matrisome proteins of different origins identified cancer cell–derived matrisome proteins as being correlated with poor patient overall survival (e.g., AGRN, SERPINB5, and CSTB), whereas stromal cell–derived proteins correlated either with good or poor survival and many showed no correlation with survival. **B–D,** Quantitative TMT MS/MS reporter-ion ratios normalized to normal pancreas in human samples show increasing amounts of AGRN (**B**), SERPINB5 (**C**), and CSTB (**D**) proteins during PDAC progression. **E–G,** Kaplan–Meier analyses of TCGA RNA-seq data show that high expression levels of *AGRN* (**E**), *SERPINB5* (**F**), and *CSTB* (**G**) correlate with poor overall patient survival. **H–J,** mRNA levels of all three genes, *Agrn* (**H**), *Serpinb5* (**I**), and *Cstb* (**J**), are significantly elevated during PDAC progression in KC/KPC mouse samples, as shown by qRT-PCR. **K–M,** IHC confirmed protein overexpression in human and mouse PDAC compared with normal samples. Arrows, epithelial regions. Scale bar, 200 μm. *, $P < 0.05$; **, $P < 0.01$; ***, $P < 0.001$; ****, $P < 0.0001$; ns, not significant. All *P* values come from two-tailed *t* tests. All columns are represented by mean ± SD. This labeling scheme applies to all related figures.

Line Encyclopedia (CCLE; Supplementary Fig. S1A–S1C). For each gene, we screened a number of gRNA guides to select one or two gRNAs that most effectively knocked down expression at both mRNA and protein level (**Fig. 2A**). We found that cells knocked down for each of the three genes grew more slowly in *in vitro* proliferation assays (Supplementary Fig. S2A).

To test the *in vivo* function of the three genes in primary tumor growth and metastasis, we orthotopically injected the control or knockdown cell lines for each gene into immunocompromised NSG mice. We found that knocking down each of the three genes significantly reduced the primary tumor weight in the case of all gRNA guides tested (**Fig. 2B**). We then monitored distant metastasis in both

Published OnlineFirst February 6, 2020; DOI: 10.1158/0008-5472.CAN-19-2578

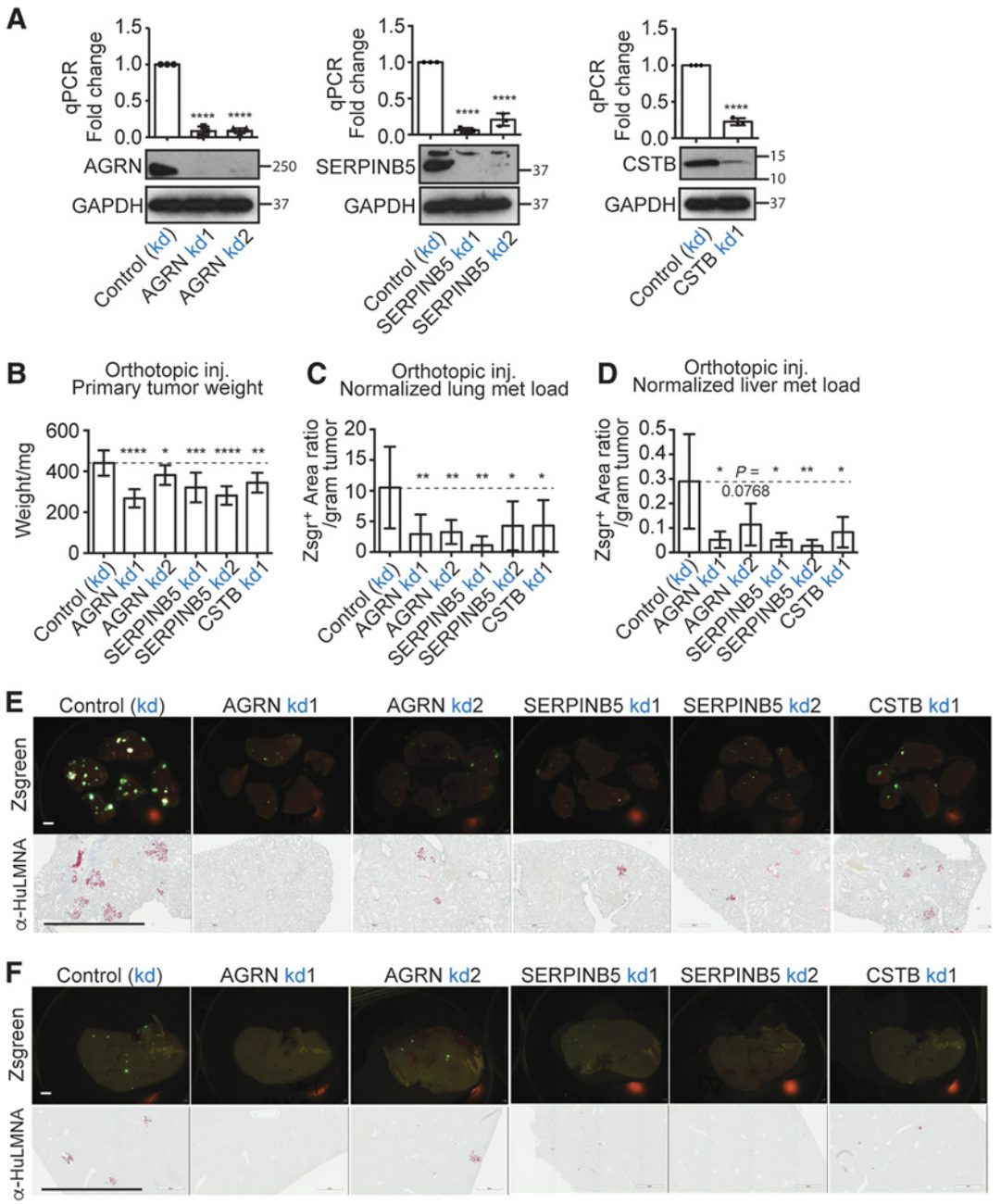

Figure 2.

Effects of knocking down expression of AGRN, SERPINB5, and CSTB on primary tumor growth and lung metastasis. **A,** CRISPR inactivation knocked down (kd) expression in the BxPC3 G1.1 cell line of AGRN, SERPINB5, and CSTB, respectively, as shown by qPCR (top) and Western blot (bottom). GAPDH was used as the loading control. Orthotopic injection of BxPC3 G1.1 cells knocked down for AGRN, SERPINB5, or CSTB showed that inhibition of each of them significantly reduced primary tumor weight (**B**), lung (**C**), and liver (**D**) metastasis load after normalization to primary tumor weight (**C**). *N* numbers are 12, 8, 9, 8, 10, 7 (left to right). Lung (**E**) and liver (**F**) metastasis images from CRISPR inactivation orthotopic xenograft mice are shown. Zsgreen (top rows) and human-specific LMNA staining (bottoms rows) both highlight cancer cells. Scale bar, 2 mm. *, $P < 0.05$; **, $P < 0.01$; ***, $P < 0.001$; ****, $P < 0.0001$.

lungs and livers. We quantified metastasis by the percentage of Zsgreen-positive area in the left pulmonary lobe (**Fig. 2C** and **D**) and also indicated metastasis by IHC with a human-specific anti-LMNA antibody, because the cancer cells are of human origin (**Fig. 2E** and **F**). We found that knocking down expression of each of the three genes led to significant decreases in the metastasis load normalized to the primary tumor weight with all gRNA guides tested in both lungs (**Fig. 2C** and **E**) and liver (**Fig. 2D** and **F**). Note that the lung-selected BxPC3 cell line is highly lung-metastatic and poorly liver-metastatic (comparing the *y*-axes in **Fig. 2C** and **D**). The liver metastases may not

Published OnlineFirst February 6, 2020; DOI: 10.1158/0008-5472.CAN-19-2578

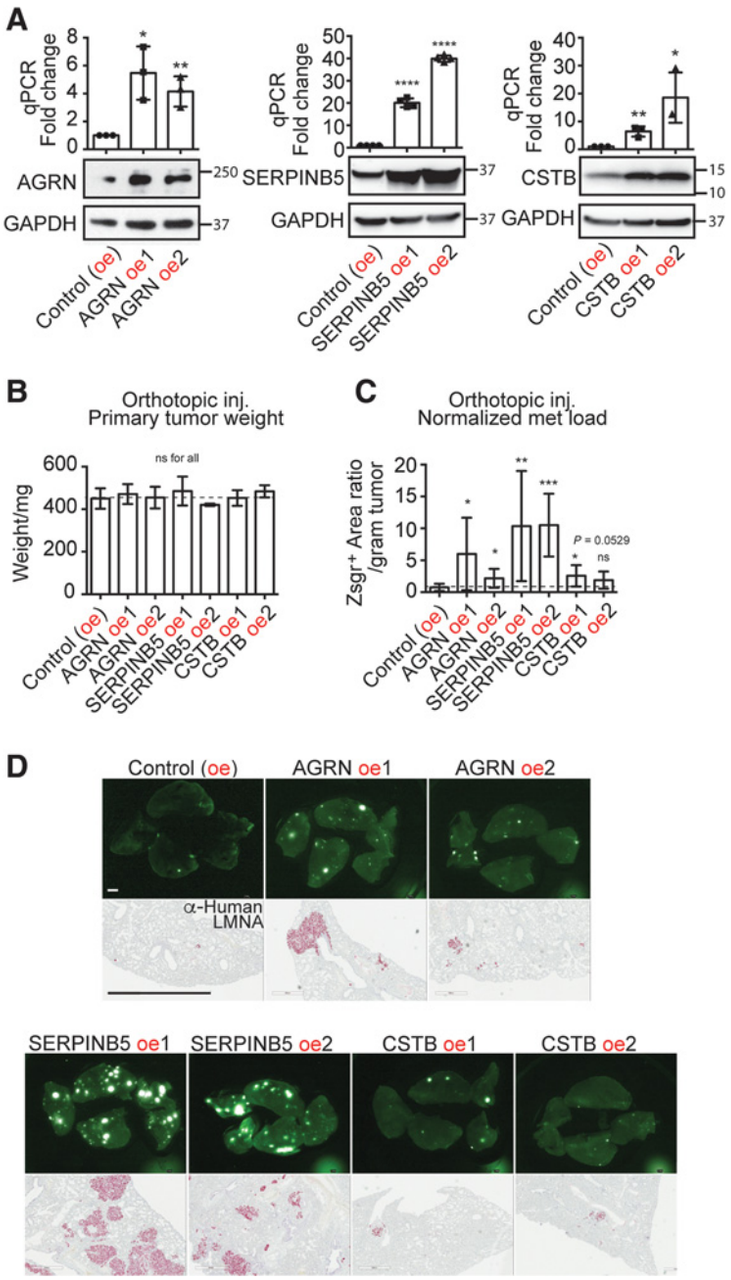

Figure 3.

Effects of overexpressing AGRN, SERPINB5, and CSTB on primary tumor growth and lung metastasis. **A,** CRISPR-SAM–induced overexpression (oe) in the AsPC1 cell line overexpressed AGRN, SERPINB5, and CSTB, respectively, as shown by qPCR (top) and Western blot (bottom). GAPDH was used as the loading control. **B** and **C,** Orthotopic injection of AsPC1 overexpressing AGRN, SERPINB5, or CSTB showed that overexpression of each of them failed to affect primary tumor weight (**B**). However, overexpression significantly increased lung metastasis load after normalization to primary tumor weight (**C**), except for CSTB oe2, for which $P = 0.0529$. *N* numbers are 8, 6, 7, 6, 5, 5, 6 (left to right). **D,** Lung images from CRISPR-SAM orthotopic xenograft mice are shown. Zsgreen (top rows) and human-specific LMNA staining (bottom rows) both highlight cancer cells. Scale bar, 2 mm. *, $P < 0.05$; **, $P < 0.01$; ***, $P < 0.001$; ****, $P < 0.0001$; ns, not significant.

all result from hematogenous/lymphatic dissemination, because there may be direct cell transfer to the liver either from primary sites, or from ascites resulting from pancreatic tumors. This set of experiments established direct roles for AGRN, SERPINB5, and CSTB in promoting PDAC growth and metastasis.

Overexpression of AGRN, SERPINB5, and CSTB in tumor cells increases metastasis

To investigate the functional roles of the three genes in a complementary experiment, we used the synergistic activation mediator (SAM) CRISPR/dCas9 gene activation system to induce expression of each of the three genes (15). The activation was performed in the AsPC1 cell line, which expresses lower levels of all three genes as compared with the BxPC3 cell line in CCLE (Supplementary Fig. S1). For each gene, we selected two gRNA guides that most effectively induced expression at both the mRNA and protein level (**Fig. 3A**). Overexpressing the AGRN and SERPINB5 by both gRNAs and CSTB by one gRNA resulted in significant increases in *in vitro* proliferation for all gRNAs tested, although compared with the knockdown set of cells, the changes in proliferation were small (Supplementary Fig. S2B). Furthermore, we found that orthotopic tumor weights from these modified cells were not different from control cells (**Fig. 3B**). The discordance between the *in vitro* proliferation assay and the *in vivo* tumor growth assay could be due to the differences between *in vitro* and *in vivo* environments, such as the interplay between cancer cells and various types of stromal cells. It is also possible that overexpressing

Published OnlineFirst February 6, 2020; DOI: 10.1158/0008-5472.CAN-19-2578

the three genes is not sufficient alone to alter primary tumor growth, or that the effects are cell line specific. We then examined lung metastasis by normalizing the fraction of Zsgreen-positive area to primary tumor weight (**Fig. 3C** and **D**). We discovered that overexpressing AGRN or SERPINB5 significantly increased lung metastasis using both guides tested for each (**Fig. 3C**). CSTB overexpression led to significantly increased metastasis with one guide, and not significantly increased metastasis with the second guide, however, the *P* value (0.0529) is very close to being significant (**Fig. 3C**). We could not quantify metastasis to the liver because liver metastasis was not evident from AsPC1 cells.

Combining the results from both knockdown and overexpression experiments, we conclude that (i) each of AGRN, SERPINB5, and CSTB is required for promotion of metastasis and can enhance metastasis to varying degrees; (ii) they may play a small role in primary tumor growth.

AGRN promotes epithelial-to-mesenchymal transition

Epithelial-to-mesenchymal transition (EMT) is known to regulate malignant cell motility, invasiveness, and dissemination to form distant metastases (21). We asked whether the cancer cell–derived proteins, AGRN, SERPINB5, and CSTB, could regulate EMT. We first confirmed by IHC that the xenograft tumors knocked down or overexpressing each of the three genes have the expected downregulation and upregulation of the corresponding proteins (Supplementary Fig. S3A and S3B). We then confirmed these changes at the RNA level using qPCR primers that amplified the cDNA only from human cells, but not from mouse tumors (Supplementary Fig. S3C, S3D and S3E).

To examine EMT, we performed double-color IHC in xenograft primary tumors knocked down or overexpressing each of the genes. Specifically, we used a human-specific anti-LMNA antibody to highlight cancer cells and quantified the percentage of $LMNA^+$ cancer cells also positive for the mesenchymal markers, ZEB1, VIM, and the epithelial marker CDH1. AGRN knocked-down (kd) tumors have reduced proportions of $ZEB1^+$, VIM^+, and increased proportions of $CDH1^+$ cancer cells (**Fig. 4A–C**), while AGRN-overexpressing tumors had the opposite phenotypes (**Fig. 4D–F**). However, knocking down and overexpressing SERPINB5 and CSTB did not have any impact on these EMT markers (**Fig. 4A–F**). We also tested the expression of additional EMT markers by species-specific qPCR. We designed human (cancer cell) sequence-specific qPCR primers to amplify additional mesenchymal markers, TWIST1, SNAI1, and FN1, in the xenograft tumor cDNA (Supplementary Fig. S4A). AGRN kd, but not knockdowns of SERPINB5 or CSTB, reduced expression of these markers (Supplementary Fig. S4B). AGRN overexpression did not appear to change expression of TWIST1 and SNAI1 by qPCR statistically significantly. Consistent with that result, AGRN overexpression also had less impact on ZEB-1, VIM, and CDH1 as compared with AGRN knockdown in the double-color IHC experiment.

Collectively, these results suggest that AGRN acts to promote EMT in primary tumors. This further implies that AGRN likely promotes metastasis partly through increasing the EMT program, which potentially regulates early metastasis steps, such as dissemination.

SERPINB5 and CSTB promote extravasation

To test whether each of the three ECM proteins influenced later steps of the metastatic cascade (survival in the circulation, extravasation, and colonization), we tested the experimental pulmonary metastasis model. Specifically, we injected cancer cells, overexpressing or knocked down for each of the three genes, directly into the circulation via the lateral tail vein. We found that knocking down each of the three genes significantly reduced lung metastasis compared to controls (**Fig. 5A**; Supplementary Fig. S5A), and overexpression of all three genes significantly increased lung metastasis (**Fig. 5B**; Supplementary Fig. S5B). This suggests that all three genes can promote later steps of metastasis.

One key step in the late metastatic cascade is extravasation. Therefore, we performed an *in vivo* extravasation assay to test whether AGRN, SERPINB5, or CSTB promote extravasation. Specifically, we inoculated the overexpression set of cells into the lateral tail vein and counted the percentage of cells that were extravascular in the lungs using confocal microscopy. We chose 24 hours after injection over later time points to minimize the effect of cell division. We discovered that AGRN-overexpressing cells were comparable with the control cells in extravasation ratio; however, both SERPINB5 and CSTB-overexpressing cells showed significantly enhanced extravasation (**Fig. 5C** and **D**). We could not perform extravasation assays on the knockdown set of BxPC3 cells because we observed that BxPC3 cells clustered together in the vasculature, making it impossible to quantify extravasation in single cells (Supplementary Fig. S5C). This is possibly due to the fact that BxPC3 cells are bigger than AsPC1 cells and therefore they do not spread well in the lung vasculature.

Invadopodia are protrusive structures expressing MMP14 (MT1-MMP), which cleaves ECM and contributes to breaching the basement membrane, and they are required for cancer cell extravasation (22, 23). We therefore tested invadopodial activity and quantified invadopodia-positive fraction in these cancer cells. Gelatin degradation assay is commonly used to test invadopodial activity. We quantified the fraction of cells that degraded gelatin, making dark spots on coverslips coated with Alexa Fluor 594–labeled gelatin, at 20 hours postplating (**Fig. 5E**). We discovered that cancer cells that overexpress SERPINB5 and CSTB were significantly better at degrading gelatin (**Fig. 5F**) compared with AGRN-overexpressing or control cells. The degradation spots colocalized with TKS5-positive invadopodia in AsPC1 cells (**Fig. 5G**; Supplementary Fig. S5D). Consistent with this correspondence, cancer cells that overexpress SERPINB5 and CSTB have significantly higher fraction of cells with $TKS5^+$ invadopodia (**Fig. 5H**; Supplementary Fig. S5E).

Invadopia utilize MMPs to degrade the ECM; in fact, invasive cancer cells secrete proteases such as MMPs and cathepsins to promote invasion (22, 23). We therefore tested the protease activity in cells that overexpress the three proteins, using fluorescein-conjugated peptides that are quenched and can be activated by protease cleavage (**Fig. 5I**; ref. 20). The substrates tested were largely cleaved by recombinant MMPs (Q3, Q6, PQ19) or serine protease uPA (PQ2), but not by ADAMs or cathepsins (**Fig. 5J**). We found that lysates from CSTB and SERPINB5 cells appear to express higher MMP but not uPA activity because they cleaved Q3, Q6, and PQ19 significantly better than did control cells, whereas AGRN did not affect the cleavage of the tested substrates (**Fig. 5K**). Supporting these assignments of substrate specificity, EDTA significantly reduced the cleavage of Q3, Q6, and PQ19, but not of PQ2. Thus, these results suggest that SERPINB5 and CSTB likely promote extravasation through promoting invadopodia formation and MMP activity.

SERPINB5 protein levels released to desmoplastic stroma correlate with poor patient survival

Kaplan–Meier survival analysis using TCGA RNA-seq data showed that high mRNA expression levels of AGRN, SERPINB5, and CSTB correlate with poor survival (**Fig. 1E–G**). We sought to investigate survival correlations at the protein level using IHC to examine

Published OnlineFirst February 6, 2020; DOI: 10.1158/0008-5472.CAN-19-2578

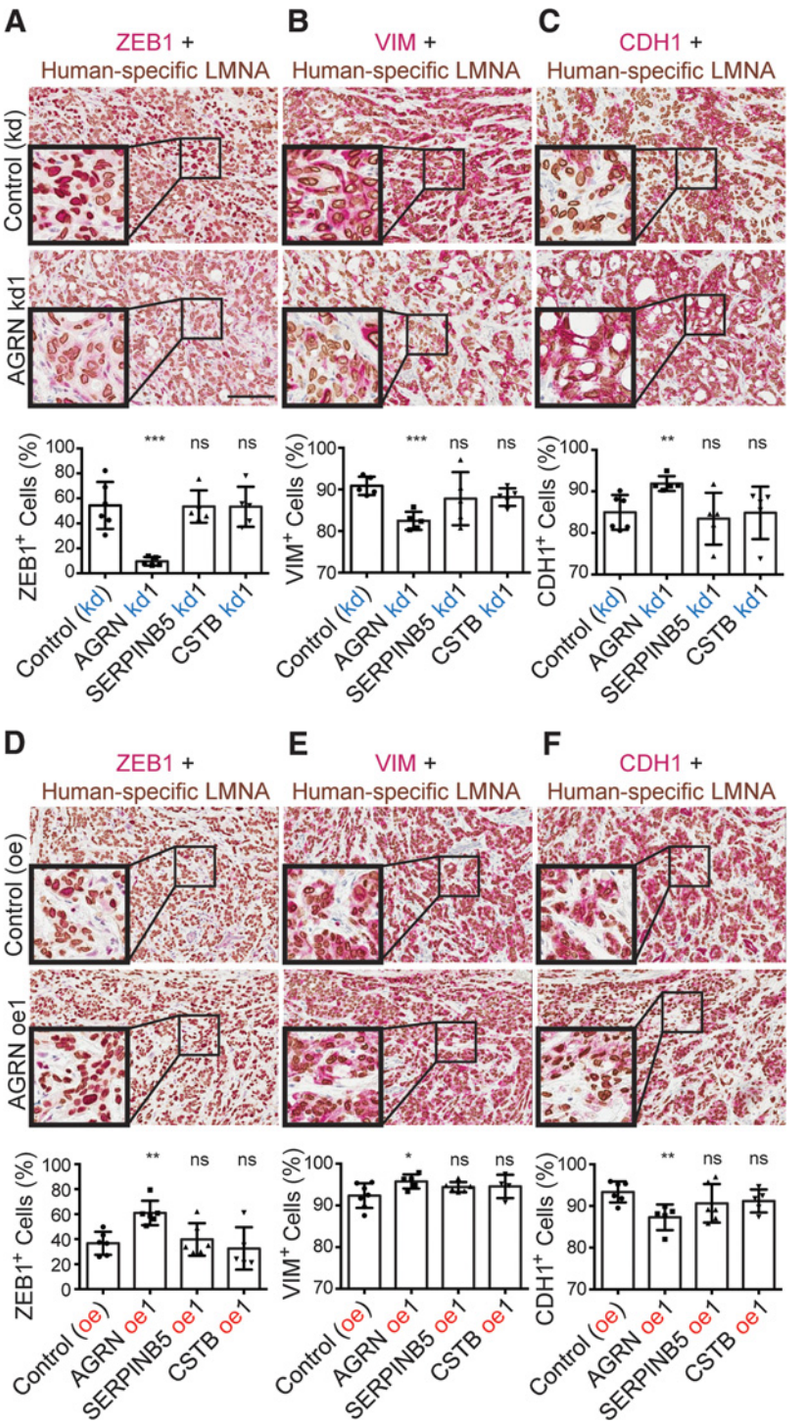

Figure 4.

AGRN promotes EMT in primary tumors. **A–F,** Double-color IHC with human-specific LMNA in brown and ZEB1 (**A** and **D**), VIM (**B** and **E**), or CDH1 (**C** and **F**) in red. The corresponding quantifications (see Materials and Methods) show that AGRN kd, but not SERPINB5 or CSTB kd, reduced ZEB1+ and VIM+ tumor-cell fractions and increased the $CDH1^+$ tumor cell fraction, while AGRN overexpression regulated EMT in the opposite direction. *, $P < 0.05$; **, $P < 0.01$; ***, $P < 0.001$; ns, not significant.

SERPINB5 protein expression on a human PDAC tumor microarray comprising samples from 75 patients. We observed SERPINB5 staining both within the epithelial cells and associated with desmoplastic stroma (**Fig. 6**; Supplementary Fig. S6A–S6C). We found that high SERPINB5 protein levels, when associated with the stroma, but not when associated with the epithelial cells, correlated with significantly poor patient survival (**Fig. 6A** and **B**; Supplementary Fig. S6A–S6C). To confirm the cellular origin of the stromally located SERPINB5 protein, we performed RNA *in situ* hybridization of SERPINB5 on clinical samples showing high stromal SERPINB5 score. We showed that SERPINB5 mRNA is exclusively present in the epithelial compartment (KRT19-positive) and is absent from cells in the desmoplastic region (**Fig. 6C**), whereas the adjacent section showed high SERPINB5 protein levels associated with the extracellular matrix (**Fig. 6D**). Therefore, the stromal SERPINB5 protein is produced by the cancer cells and deposited into the extracellular stroma in some

Published OnlineFirst February 6, 2020; DOI: 10.1158/0008-5472.CAN-19-2578

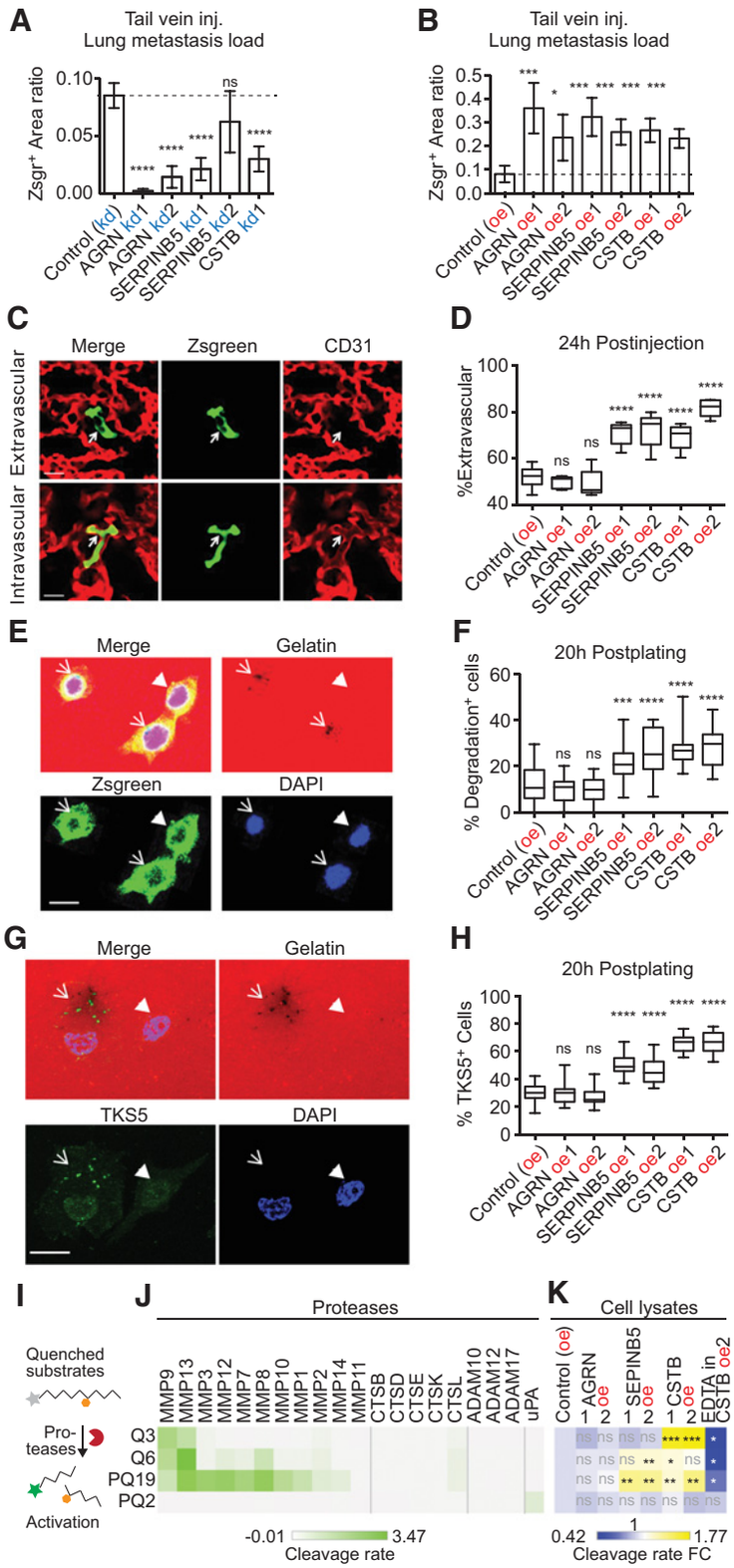

Figure 5.

SERPINB5 and CSTB promote formation of invadopodia and extravasation. **A** and **B,** Tail-vein injection showed that knockdown (kd; **A**) of each of the three genes restricted, while overexpression (oe; **B**) of each promoted experimental metastasis. $N = 5$ for all. **C,** Example images of cells that are inside or outside of vasculature 24 hours after tail-vein injection. Arrows, cancer cells that are Zsgreen-positive. **D,** Extravasation assay shows that overexpression of either SERPINB5 or CSTB (but not AGRN) caused a higher fraction of cancer cells to be extravasated at 24 hours postinjection. At least 40 cells were scored blindly per mouse. $N = 5$ for all, except that $N = 10$ for control group. **E,** Example images of cells that degraded (arrows) or did not degrade (arrowhead) gelatin in the course of invadopodial assays. **F,** Quantification of percentage of cells per field that have degraded gelatin at 20 hours postplating for each cell line. **G,** Colocalization of TKS5$^+$ invadopodia and the degradation spots in AsPC1 cells that degraded (arrow) or did not degrade (arrowhead) gelatin 20 hours postplating. **H,** Quantification of percentage of cells per field that have TKS5$^+$ invadopodia at 20 hours post-plating for each cell line. At least 20 fields were quantified per cell line for **F** and **H** (see Materials and Methods). **I,** Protease activity assay uses peptides with quenched fluorescein that can be dequenched by protease cleavage. Four peptides were cleaved by recombinant proteases (**J**) or cell lysates (**K**) in triplicate. Average cleavage rate is illustrated (**J**) and compared with the control cell lines (**K**). *, $P < 0.05$; ***, $P < 0.001$; ****, $P < 0.0001$; ns, not significant.

Published OnlineFirst February 6, 2020; DOI: 10.1158/0008-5472.CAN-19-2578

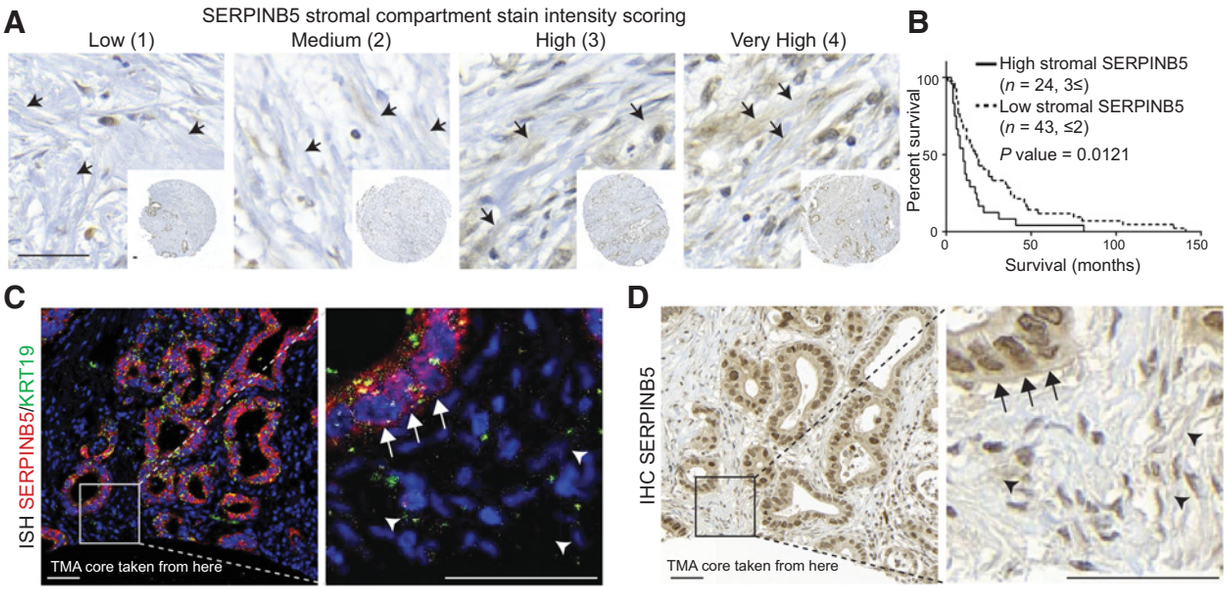

Figure 6.

Cancer cell–derived SERPINB5 is a poor prognostic factor. **A,** Representative images for stromal SERPINB5 staining scoring system on a human patient tissue microarray. Arrows, representative stromal regions that look like ECM, where the scoring was done. **B,** Survival curves from patients categorized into two populations based on high and low stromal staining showed that high stromal signal correlates with significantly poorer patient survival. **C** and **D,** RNA *in situ* hybridization showed exclusively epithelial-cell origin of SERPINB5 RNA (**C**), whereas the adjacent section (**D**), which was stained for SERPINB5 by IHC, showed protein staining over the extracellular ECM (**D**). Arrows, epithelial compartment; arrowheads, IHC signal over the ECM. Scale bars, 50 μm.

regions of PDAC tumors but not others. Supporting this secretion hypothesis, we identified SERPINB5 protein in the conditioned media from SERPINB5-overexpressing BxPC3 cells (Supplementary Fig. S6D). Our SERPINB5 human TMA results are consistent with our previous xenograft MS data that SERPINB5 protein is exclusively made by cancer cells and conform with our *in vivo* finding that SERPINB5 appears to be a metastasis promoter in PDAC.

Discussion

Cancer cell–derived matrisome proteins promote cancer progression

PDAC is known for its abundant ECM. Methods to deplete the bulk matrix in PDAC have not led to successful outcomes. Tumor microenvironment includes many types of cells, including different fibroblasts, immune cells, endothelial cells, fat cells, and neuronal cells, all of which could deposit matrisome proteins. It has long been known that fibroblasts deposit ECM proteins; however, it has only recently become evident that cancer cells also express many matrisome proteins during cancer progression and in various stress conditions and can play important roles in enhancing tumor progression (24). In our prior study, we identified a large number of cancer cell–derived matrisome proteins elevated during PDAC progression, and showed that high expression of these tumor cell–derived proteins correlates with poor patient survival (13). In this study we investigated whether these matrisome proteins play causal roles in PDAC tumorigenesis. We selected three cancer-cell-derived matrisome proteins, AGRN, SERPINB5, and CSTB, which are overrepresented in the PDAC ECM and performed *in vivo* functional analyses. We demonstrated that all three could promote metastasis at different steps of the metastatic cascade based on consistent results from both overexpression and knockdown experiments.

The overexpression experiments used the BxPC3 cell line that is KRAS wild-type and SMAD4 mutant whereas the knockdown experiments were done in the AsPC1 cell line that is KRAS mutant and SMAD4 wild-type. Thus AGRN, SERPINB5, and CSTB apparently promote metastasis independent of which signaling pathways (KRAS or SMAD4/TGFβ) initiate metastasis. These three proteins likely represent downstream players common to both initiating stimuli.

To understand how cancer cells extravasate from vasculature, for some assays (e.g., extravasation), we used a tail-vein injection model, which primarily assesses metastasis to the lungs. However, lung is a less preferred metastatic site in PDAC patients as compared with the liver. Patients with first site of lung recurrence had a more favorable outcome compared with patients who recurred with liver metastasis as the first site of recurrence (25). Therefore, it is possible that cells metastasizing to the lung and liver use somewhat different mechanisms. The results of our orthotopic metastasis assays suggest that the three genes we have studied promote metastasis to both the lungs and the liver from the orthotopic site; however, the mechanisms of the latter metastatic cascade will need to be directly studied in the liver.

There are other examples of cancer cell–derived matrisome proteins playing a role in tumorigenesis. Drug-resistant breast cancer cells significantly upregulate ECM components, which are hypothesized to provide protection to cancer cells (26). Circulating tumor cells (CTC) in PDAC exhibit a very high expression of ECM proteins (27). The functional consequences of some of the cancer cell–expressed matrisome proteins have been implicated in cancers. For example, cancer cell–derived glycoprotein tenascin-C (TNC) initiates seeding of metastases before stroma-derived TNC takes over in breast cancer (10), and is further demonstrated to play positive roles in tumorigenesis and metastasis in multiple types of cancer, including melanoma and lung cancer (28, 29). High SPARC expression in PDAC CTCs promotes cancer cell migration and invasiveness (27). Studies from our

Published OnlineFirst February 6, 2020; DOI: 10.1158/0008-5472.CAN-19-2578

laboratory identified cancer cell- vs. stromal cell–derived matrisome proteins by mass spectrometry in breast cancer, colon cancer, melanoma, and PDAC (7, 8, 30). We see repeated overrepresentation of certain cancer cell–derived proteins across different cancer types, such as Laminin-332, some annexins, and some S100 proteins. Many of them have not been studied before and may play instrumental roles in cancer progression as the three genes (AGRN, SERPINB5, and CSTB) that we studied here.

Together, the results from this study and our previous study as discussed above suggest that increased levels of tumor cell–derived matrisome proteins could function to drive more aggressive tumor cell behaviors. Therefore, instead of the bulk matrix, cancer cell–derived matrisome proteins, or their regulators, may be more valuable targets for therapeutic interventions.

AGRN is a promoter of metastasis in PDAC

The heparin sulfate proteoglycan agrin is a basement-membrane component, best known for organizing postsynaptic differentiation at the neuromuscular junction. Recently, AGRN has been reported to be upregulated in hepatocellular carcinoma (HCC), as well as other types of cancer (31, 32). In HCC, AGRN has been shown to be secreted from human hepatic stellate cells upon activation by platelet-derived growth factor (PDGF) and to relay mechanosensitive signals into cells to regulate focal adhesion kinase and promote EMT, proliferation, migration, and invasion (31–33).

We report here that AGRN is overrepresented in the ECM of human and murine PDAC samples. Using our previously published MS dataset that allows assignment of cellular origin (epithelial tumor cell or microenvironmental stromal cell), we found that AGRN is produced predominantly by the tumor cells (about 25-fold more than stromal cell–derived AGRN; ref. 13). AGRN knockdown in the tumor cells reduced primary tumor growth moderately but significantly. However, overexpressing AGRN had no effect on primary tumor growth. In both knockdown and overexpression scenarios, AGRN levels were consistently correlated with metastatic potential. AGRN potentially promotes metastasis at multiple steps in the metastatic cascade. First, AGRN likely promotes metastasis through stimulation of the EMT program in the primary tumor, which could lead to increased migration, invasion, and dissemination of cancer cells from primary tumor sites. Consistent with our study, AGRN in cultured HCC cells has been shown to form a complex with Lrp4 and Musk, and this complex activates the FAK pathway, which drives the EMT program (32). In other systems, FAK has been shown to promote EMT by transcriptional regulation of several mesenchymal markers and delocalization of E-cadherin (34). Second, because AGRN promotes pulmonary metastasis after tail-vein injection, yet with no impact on the extravasation rate, AGRN could promote some later steps in the metastasis, such as colonization and outgrowth, which may also involve the EMT program. In support of this hypothesis, we found that AGRN promoted cancer cell ZEB-1 expression *in vivo* and it has been shown that ZEB-1 knockout PDAC cells from Pdx1-cre; $Kras^{LSL.G12D/+}$; $Tp53^{LSL.R172H/+}$; $Zeb1^{fl/fl}$ (KPCZ) mouse have reduced capacity for lung colonization, stemness, and experimental metastasis capacity (35). Therefore, AGRN promotes metastasis potentially through driving EMT and enhancing other steps in the metastatic cascade.

SERPINB5 is a promoter of metastasis in PDAC

SERPINB5, also known as Maspin, is a noninhibitory member of the serine protease inhibitor superfamily. There are conflicting reports as to whether SERPINB5 promotes or suppresses cancer. First, SERPINB5 expression can increase or decrease in cancers in a context-dependent fashion. It is downregulated in several types of cancers, including breast and prostate cancer and melanoma, and upregulated in several other types of cancers, including PDAC, gallbladder, thyroid, and colorectal cancers (36, 37). Second, there are conflicting data regarding correlation of SERPINB5 expression with clinical outcomes and prognostic implications in multiple types of cancers, such as breast cancer, thyroid, gastric, and colorectal cancers (37). SERPINB5 was traditionally identified as a tumor suppressor and was shown to inhibit cancer cell migration, invasion, and to induce apoptosis largely in breast cancer models (37). However, the *in vivo* function of SERPINB5 has not been studied in cancer contexts where SERPINB5 is upregulated.

In PDAC, SERPINB5 expression is observed in PanINs and PDAC, but not in normal pancreas (38, 39), meanwhile SERPINB5 overexpression correlates with worse prognosis in patients with PDAC (38, 40). Here we first confirmed that SERPINB5 is overrepresented at both RNA and protein level in human and mouse PDAC. We then demonstrated using both overexpression and knockdown systems that SERPINB5 promotes both spontaneous and experimental PDAC metastases, at least partially through enhancing invadopodia formation, tumor cell extravasation and potentially MMP activity. Concordant with our data, SERPINB5 mRNA level positively correlated with metastasis potential in a panel of PDAC cell lines (41). *In vitro*, SERPINB5 overexpression led to more invasive PDAC cancer cells (42). Therefore, in PDAC, SERPINB5 functions as a metastasis promoter.

SERPINB5 was suggested to be secreted and deposited in the ECM in normal mammary epithelial cells (37, 43). However, survival correlation studies were carried out only on intracellular SERPINB5 in cancers (13). How extracellular SEPRINB5 may correlate with patient outcome has not been studied. Here, we demonstrated that high SERPINB5 staining of the desmoplastic stroma is a poor prognostic indicator in PDAC human patients. We further showed that SERPINB5 mRNA is exclusively made by the epithelial cells. Consistently, our previous MS analysis discovered SERPINB5 as exclusively produced by cancer cells and it is the second most abundant PDAC cancer-cell-derived SERPIN out of ten total SERPINs identified in the enriched ECM of xenograft tumors (13). SERPINB5 protein may arrive at the non-epithelial compartment through a variety of routes, such as secretion or being passively released from dying cancer cells. Supporting the secretion hypothesis, SERPINB5 protein is detected in the conditioned media of BxPC3 PDAC cells overexpressing SERPINB5. More studies need to be carried out to understand the functions of SERPINB5 in the (extra)cellular compartment and the correlation between SERPINB5 localization and survival in PDAC and other types of cancers.

CSTB also promotes metastasis in PDAC

CSTB (cystatin B) is a cysteine protease inhibitor of the cystatin superfamily. Dysregulated expression of CSTB has been implicated in various cancers such as HCC and ovarian clear cell carcinoma (44, 45). CSTB seems to play different roles in different types of cancer. CSTB deficiency reduces primary tumor growth via sensitization of tumor cells to oxidative stress in the PyMT murine mammary cancer model (46). In contrast, CSTB downregulation could promote cell proliferation and migration in a gastric cancer cell line (47). CSTB is known to be an inhibitor of cathepsin proteases, which are frequently upregulated in multiple types of cancer (48). Increased cathepsin expression generally correlates with increased malignancy and poor patient prognosis, however, individual cathepsins may have

Published OnlineFirst February 6, 2020; DOI: 10.1158/0008-5472.CAN-19-2578

context-dependent tumor-suppressing roles (48). For example, CTSL serves as a negative prognostic marker while CSTB serves as a positive prognostic marker in patients with head and neck cancer (49). CSTB also has cathepsin-independent functions. CSTB deficiency sensitizes thymocytes to staurosporine-induced apoptosis and this function of CSTB is independent of cysteine cathepsins (50).

In our study, we found that CSTB promoted extravasation from the lung vasculature, leading to increased metastatic load in a tail-vein metastasis model. The increased extravasation rate may be due to the increased invadopodia formation observed upon CSTB overexpression. Consistent with the enhanced invadopodia formation, we observed increased cellular proteolytic activity that most likely belongs to the MMP family. Further investigation is required as to how CSTB promotes invadopodia formation and promotes metastasis, and whether such function requires inhibition of cathepsins, and if so, which cathepsins. Our previous TMT-MS data revealed some consistently overrepresented cathepsins in both human and mouse PDAC, including CTSB, CTSC, CTSD, CTSF, CTSG, CTSK, CTSL, and CTSS (13). They could be CSTB candidate targets and that should be further investigated.

We describe here functional *in vivo* characterization following up our previous comprehensive proteomic study of PDAC ECM, which suggested that, unlike stromal cell–derived matrisome proteins, cancer cells selectively upregulate matrisome proteins that correlate with poor patient outcomes. In this study, we selected three proteins, whose functional implications in PDAC have not been previously studied *in vivo*. We provide *in vivo* data that all three are metastasis promoters and function in distinct steps of the metastatic cascade. These mechanistic studies of these three proteins not only provide novel insights into their biological roles in PDAC, but also support the notion that cancer cell–derived matrisome proteins are protumorigenic and are potentially better therapeutic targets that may not lead to the same adverse effects as does nonselectively depletion of the bulk matrix.

Disclosure of Potential Conflicts of Interest

No potential conflicts of interest were disclosed.

Authors' Contributions

Conception and design: C. Tian, D. Öhlund, R.O. Hynes

Development of methodology: C. Tian, D. Öhlund, S. Rickelt, L. Hao

Acquisition of data (provided animals, acquired and managed patients, provided facilities, etc.): C. Tian, D. Öhlund, S. Rickelt, T. Lidström, Y. Huang, L. Hao, R.T. Zhao, O. Franklin, D.A. Tuveson

Analysis and interpretation of data (e.g., statistical analysis, biostatistics, computational analysis): C. Tian, D. Öhlund, T. Lidström, L. Hao, R.T. Zhao, R.O. Hynes

Writing, review, and/or revision of the manuscript: C. Tian, D. Öhlund, T. Lidström, R.O. Hynes

Administrative, technical, or material support (i.e., reporting or organizing data, constructing databases): D. Öhlund, S. Rickelt, Y. Huang, R.T. Zhao, O. Franklin

Study supervision: C. Tian, S.N. Bhatia, D.A. Tuveson, R.O. Hynes

Acknowledgments

We thank the Hope Babette Tang Histology Facility at the Koch Institute Swanson Biotechnology Center for technical assistance, David Benjamin for help with ImageJ quantification, Roderick Bronson for pathologic analysis, and Anette Berglund for technical assistance. C. Tian was a Sherry and Alan Leventhal Family Fellow of the Damon Runyon Cancer Research Foundation. This work was supported by the STARR Cancer Consortium (to R.O. Hynes and D.A. Tuveson), the Howard Hughes Medical Institute, of which R.O. Hynes was an investigator, and the Lustgarten Foundation, where D.A. Tuveson is a distinguished scholar and Director of the Lustgarten Foundation-designated Laboratory of Pancreatic Cancer Research. Support was also provided by NCI Cancer Center Support Grants to MIT, Koch Institute (P30CA14051-45) and Cold Spring Harbor (P30CA45508-27), and shared resources of the St. Giles Foundation Microscopy Center, Animal and Tissue Imaging, and the Animal Facility, both at Cold Spring Harbor Laboratory. D.A. Tuveson is also supported by the Cold Spring Harbor Laboratory Association, the NIH (5P30CA45508-27, 1U10CA180944-04, and 1R01CA190092-04, 5P20CA192996-03, 1U01CA210240-01A1), the DOD (W81XWH-13-PRCRP-IA), and the V Foundation. S. Rickelt and C. Tian were supported by postdoctoral fellowships from the MIT Ludwig Center for Molecular Oncology. D. Öhlund was supported by the Swedish Research Council (537-2013-7277 and 2017-01531), the Kempe Foundations (JCK-1301), the Swedish Society of Medicine (SLS-326921, SLS-250831, SLS- 175991, and SLS-591551), federal funds through the county council of Västerbotten (ALFVLL369081, VLL-643451), the Cancer Research Foundation in Northern Sweden (AMP15-793 and AMP17-877), the Swedish Foundation for International Cooperation in Research and Higher Education (PT2015-6432), the Knut and Alice Wallenberg Foundation, and the Swedish Cancer Society (CAN 2017/332 and CAN 2017/827). This study was also supported in part by a Koch Institute support grant no. P30-CA14051 from the NCI (Swanson Biotechnology Center), and a Core Center grant P30-ES002109 from the National Institute of Environmental Health Sciences, the Ludwig Fund for Cancer Research, and the Koch Institute's Marble Center for Cancer Nanomedicine. S.N. Bhatia is a Howard Hughes Medical Institute Investigator.

The costs of publication of this article were defrayed in part by the payment of page charges. This article must therefore be hereby marked *advertisement* in accordance with 18 U.S.C. Section 1734 solely to indicate this fact.

Received August 23, 2019; revised December 20, 2019; accepted January 30, 2020; published first February 6, 2020.

References

1. Siegel RL, Miller KD, Jemal A. Cancer statistics, 2019. CA Cancer J Clin 2019;69:7–34.
2. Manji GA, Olive KP, Saenger YM, Oberstein P. Current and emerging therapies in metastatic pancreatic cancer. Clin Cancer Res 2017;23:1670–8.
3. Cid-Arregui A, Juarez V. Perspectives in the treatment of pancreatic adenocarcinoma. World J Gastroenterol 2015;21:9297–316.
4. Rhim AD, Oberstein PE, Thomas DH, Mirek ET, Palermo CF, Sastra SA, et al. Stromal elements act to restrain, rather than support, pancreatic ductal adenocarcinoma. Cancer Cell 2014;25:735–47.
5. Ozdemir BC, Pentcheva-Hoang T, Carstens JL, Zheng X, Wu CC, Simpson TR, et al. Depletion of carcinoma-associated fibroblasts and fibrosis induces immunosuppression and accelerates pancreas cancer with reduced survival. Cancer Cell 2014;25:719–34.
6. Amakye D, Jagani Z, Dorsch M. Unraveling the therapeutic potential of the Hedgehog pathway in cancer. Nat Med 2013;19:1410–22.
7. Naba A, Clauser KR, Lamar JM, Carr SA, Hynes RO. Extracellular matrix signatures of human mammary carcinoma identify novel metastasis promoters. Elife 2014;3:e01308.
8. Naba A, Clauser KR, Hoersch S, Liu H, Carr SA, Hynes RO. The matrisome: *in silico* definition and *in vivo* characterization by proteomics of normal and tumor extracellular matrices. Mol Cell Proteomics 2012;11:M111.014647.
9. Pickup MW, Mouw JK, Weaver VM. The extracellular matrix modulates the hallmarks of cancer. EMBO Rep 2014;15:1243–53.
10. Oskarsson T, Acharyya S, Zhang XHF, Vanharanta S, Tavazoie SF, Morris PG, et al. Breast cancer cells produce tenascin C as a metastatic niche component to colonize the lungs. Nat Med 2011;17:867–74.
11. Malanchi I, Santamaria-Martinez A, Susanto E, Peng H, Lehr HA, Delaloye JF, et al. Interactions between breast cancer stem cells and their niche govern metastatic colonization of the lung. Nature 2012;48:S15.
12. Socovich AM, Naba A. The cancer matrisome: from comprehensive characterization to biomarker discovery. Semin Cell Dev Biol 2019;89:157–66.
13. Tian C, Clauser KR, Ohlund D, Rickelt S, Huang Y, Gupta M, et al. Proteomic analyses of ECM during pancreatic ductal adenocarcinoma progression reveal different contributions by tumor and stromal cells. Proc Natl Acad Sci U S A 2019;116:19609–18.

14. Boj SF, Hwang CI, Baker LA, Chio II, Engle DD, Corbo V, et al. Organoid models of human and mouse ductal pancreatic cancer. Cell 2015;160:324–38.
15. Konermann S, Brigham MD, Trevino AE, Joung J, Abudayyeh OO, Barcena C, et al. Genome-scale transcriptional activation by an engineered CRISPR-Cas9 complex. Nature 2015;517:583–8.
16. Gilbert LA, Horlbeck MA, Adamson B, Villalta JE, Chen Y, Whitehead EH, et al. Genome-scale CRISPR-mediated control of gene repression and activation. Cell 2014;159:647–61.
17. Sharma VP, Entenberg D, Condeelis J. High-resolution live-cell imaging and time-lapse microscopy of invadopodium dynamics and tracking analysis. Methods Mol Biol 2013;1046:343–57.
18. Baik M, French B, Chen YC, Byers JT, Chen KT, French SW, et al. Identification of invadopodia by TKS5 staining in human cancer lines and patient tumor samples. MethodsX 2019;6:718–26.
19. Bailey P, Chang DK, Nones K, Johns AL, Patch AM, Gingras MC, et al. Genomic analyses identify molecular subtypes of pancreatic cancer. Nature 2016;531: 47–52.
20. Dudani JS, Ibrahim M, Kirkpatrick J, Warren AD, Bhatia SN. Classification of prostate cancer using a protease activity nanosensor library. Proc Natl Acad Sci U S A 2018;115:8954–9.
21. Brabletz T, Kalluri R, Nieto MA, Weinberg RA. EMT in cancer. Nat Rev Cancer 2018;18:128–34.
22. Leong HS, Robertson AE, Stoletov K, Leith SJ, Chin CA, Chien AE, et al. Invadopodia are required for cancer cell extravasation and are a therapeutic target for metastasis. Cell Rep 2014;8:1558–70.
23. Weaver AM. Invadopodia: specialized cell structures for cancer invasion. Clin Exp Metastasis 2006;23:97–105.
24. Gao-Feng Xiong RX. Function of cancer cell-derived extracellular matrix in tumor progression. J Cancer Metastasis Treat 2016;2:357–64.
25. Sahin IH, Elias H, Chou JF, Capanu M, O'Reilly EM. Pancreatic adenocarcinoma: insights into patterns of recurrence and disease behavior. BMC Cancer 2018;18: 769.
26. Iseri OD, Kars MD, Arpaci F, Gunduz U. Gene expression analysis of drug-resistant MCF-7 cells: implications for relation to extracellular matrix proteins. Cancer Chemother Pharmacol 2010;65:447–55.
27. Ting DT, Wittner BS, Ligorio M, Vincent Jordan N, Shah AM, Miyamoto DT, et al. Single-cell RNA sequencing identifies extracellular matrix gene expression by pancreatic circulating tumor cells. Cell Rep 2014;8:1905–18.
28. Gocheva V, Naba A, Bhutkar A, Guardia T, Miller KM, Li CM, et al. Quantitative proteomics identify Tenascin-C as a promoter of lung cancer progression and contributor to a signature prognostic of patient survival. Proc Natl Acad Sci U S A 2017;114:E5625–E34.
29. Lowy CM, Oskarsson T. Tenascin C in metastasis: a view from the invasive front. Cell Adh Migr 2015;9:112–24.
30. Naba A, Clauser KR, Whittaker CA, Carr SA, Tanabe KK, Hynes RO. Extracellular matrix signatures of human primary metastatic colon cancers and their metastases to liver. BMC Cancer 2014;14:518.
31. Chakraborty S, Njah K, Pobbati AV, Lim YB, Raju A, Lakshmanan M, et al. Agrin as a mechanotransduction signal regulating YAP through the Hippo pathway. Cell Rep 2017;18:2464–79.
32. Chakraborty S, Lakshmanan M, Swa HL, Chen J, Zhang X, Ong YS, et al. An oncogenic role of Agrin in regulating focal adhesion integrity in hepatocellular carcinoma. Nat Commun 2015;6:6184.
33. Lv X, Fang C, Yin R, Qiao B, Shang R, Wang J, et al. Agrin para-secreted by PDGF-activated human hepatic stellate cells promotes hepatocarcinogenesis in vitro and in vivo. Oncotarget 2017;8:105340–55.
34. Yoon H, Dehart JP, Murphy JM, Lim ST. Understanding the roles of FAK in cancer: inhibitors, genetic models, and new insights. J Histochem Cytochem 2015;63:114–28.
35. Krebs AM, Mitschke J, Lasierra Losada M, Schmalhofer O, Boerries M, Busch H, et al. The EMT-activator Zeb1 is a key factor for cell plasticity and promotes metastasis in pancreatic cancer. Nat Cell Biol 2017;19:518–29.
36. Berardi R, Morgese F, Onofri A, Mazzanti P, Pistelli M, Ballatore Z, et al. Role of maspin in cancer. Clin Transl Med 2013;2:8.
37. Bodenstine TM, Seftor RE, Khalkhali-Ellis Z, Seftor EA, Pemberton PA, Hendrix MJ. Maspin: molecular mechanisms and therapeutic implications. Cancer Metastasis Rev 2012;31:529–51.
38. Cao D, Zhang Q, Wu LS, Salaria SN, Winter JW, Hruban RH, et al. Prognostic significance of maspin in pancreatic ductal adenocarcinoma: tissue microarray analysis of 223 surgically resected cases. Mod Pathol 2007;20:570–8.
39. Maass N, Hojo T, Ueding M, Luttges J, Kloppel G, Jonat W, et al. Expression of the tumor suppressor gene Maspin in human pancreatic cancers. Clin Cancer Res 2001;7:812–7.
40. Lim YJ, Lee JK, Jang WY, Song SY, Lee KT, Paik SW, et al. Prognostic significance of maspin in pancreatic ductal adenocarcinoma. Korean J Intern Med 2004;19: 15–8.
41. Mardin WA, Petrov KO, Enns A, Senninger N, Haier J, Mees ST. SERPINB5 and AKAP12 - expression and promoter methylation of metastasis suppressor genes in pancreatic ductal adenocarcinoma. BMC Cancer 2010;10:549.
42. Hong SN, Lee JK, Choe WH, Ha HY, Park K, Sung IK, et al. The effect of aberrant maspin expression on the invasive ability of pancreatic ductal adenocarcinoma cells. Oncol Rep 2009;21:425–30.
43. Khalkhali-Ellis Z, Hendrix MJ. Elucidating the function of secreted maspin: inhibiting cathepsin D-mediated matrix degradation. Cancer Res 2007;67: 3535–9.
44. Takaya A, Peng WX, Ishino K, Kudo M, Yamamoto T, Wada R, et al. Cystatin B as a potential diagnostic biomarker in ovarian clear cell carcinoma. Int J Oncol 2015;46:1573–81.
45. Lin YY, Chen ZW, Lin ZP, Lin LB, Yang XM, Xu LY, et al. Tissue levels of stefin A and stefin B in hepatocellular carcinoma. Anat Rec 2016;299:428–38.
46. Butinar M, Prebanda MT, Rajkovic J, Jeric B, Stoka V, Peters C, et al. Stefin B deficiency reduces tumor growth via sensitization of tumor cells to oxidative stress in a breast cancer model. Oncogene 2014;33:3392–400.
47. Zhang J, Shi Z, Huang J, Zou X. CSTB downregulation promotes cell proliferation and migration and suppresses apoptosis in gastric cancer SGC-7901 cell line. Oncol Res 2016;24:487–94.
48. Olson OC, Joyce JA. Cysteine cathepsin proteases: regulators of cancer progression and therapeutic response. Nat Rev Cancer 2015;15:712–29.
49. Budihna M, Strojan P, Smid L, Skrk J, Vrhovec I, Zupevc A, et al. Prognostic value of cathepsins B, H, L, D and their endogenous inhibitors stefins A and B in head and neck carcinoma. Biol Chem Hoppe Seyler 1996;377:385–90.
50. Kopitar-Jerala N, Schweiger A, Myers RM, Turk V, Turk B. Sensitization of stefin B-deficient thymocytes towards staurosporin-induced apoptosis is independent of cysteine cathepsins. FEBS Lett 2005;579:2149–55.

Cancer Research
The Journal of Cancer Research (1916–1930) | The American Journal of Cancer (1931–1940)

AACR American Association for Cancer Research

Cancer Cell–Derived Matrisome Proteins Promote Metastasis in Pancreatic Ductal Adenocarcinoma

Chenxi Tian, Daniel Öhlund, Steffen Rickelt, et al.

Cancer Res 2020;80:1461-1474. Published OnlineFirst February 6, 2020.